

# Coulomb versus nuclear break-up of $^{11}\text{Be}$ halo nucleus in a non perturbative framework.

M.Fallot<sup>a)</sup>, J.A.Scarpaci<sup>a)</sup>, D.Lacroix<sup>b)</sup>, Ph.Chomaz<sup>c)</sup> and J.Margueron<sup>a)</sup>

<sup>a)</sup> *Institut de Physique Nucléaire, IN2P3-CNRS, 91406 Orsay, France*

<sup>b)</sup> *LPC/ISMRA, Blvd du Maréchal Juin, 14050 Caen, France*

<sup>c)</sup> *G.A.N.I.L., B.P. 5027, F-14076 Caen Cedex 5, France*

The  $^{11}\text{Be}$  break-up is calculated using a non perturbative time-dependent quantum calculation. The evolution of the neutron halo wave function shows an emission of neutron at large angles for grazing impact parameters and at forward angles for large impact parameters. The neutron angular distribution is deduced for the different targets and compared to experimental data. We emphasize the diversity of diffraction mechanisms, in particular we discuss the interplay of the nuclear effects such as the towing mode and the Coulomb break-up. A good agreement is found with experimental data.

(January 30, 2020)

**PACS:** 21.60.-n; 24.50.+g; 25.60.-t; 24.10.-i

**Keywords:** reaction mechanisms, halo nuclei, non-perturbative calculations .

## I. INTRODUCTION

A major breakthrough of the last decade in nuclear physics is the discovery of halo nuclei [1]. The presence of these extended systems has been uncovered by break-up studies. However, an unambiguous interpretation of these reactions requires a deep understanding of reaction mechanisms such as diffractive effects [2]. In particular, the interplay between nuclear and Coulomb dissociation is of major importance.

On the experimental side, measurements of the neutron angular distribution have been performed for the one-neutron break-up of  $^{11}\text{Be}$  on Au, Ti and Be targets [3]. They clearly present two contributions. One peaked at small angles (below 10 degrees) which strongly varies with the target ; for the Au target the cross section is as high as 50 barns per steradian at small angles whereas for the Be target it is around 1 barn per steradian. A second one located at large angles which shows a lesser dependence with the target ; the cross section around 30 degrees is about 100 mbarn per steradian for all studied targets. The small angle region was understood through models based on Coulomb-excitation theory to come from Coulomb dissociation [3] and the large angle emission was thought to be a consequence of nuclear break-up. At present, either perturbative method [4,5] including both interactions or non perturbative calculations [6,7] which only account for the Coulomb field have been performed so far. In this article, we present a three-dimensional non-perturbative time-dependent model which accounts both for the Coulomb and the nuclear effects.

Our calculation shows that this large angle emission is due to the interaction of the particle with the nuclear potential. Such an emission has already been observed in reactions between stable nuclei [8] and was called "towing mode" as the particle is pulled out from the target and towed by the projectile for a short while. We predicted the emission to the continuum of particles coming from the target with specific angles and energies in agreement with the measurements [9].

In the following, we will show through our calculation that both Coulomb and nuclear fields play an important role in the case of the neutron break-up of halo nuclei.

## II. DESCRIPTION AND INPUTS OF THE MODEL

We use the calculation presented in a previous paper [8] and apply it to the reactions  $^{197}\text{Au}$ ,  $^{48}\text{Ti}$ ,  $^9\text{Be}$  ( $^{11}\text{Be}$ ,  $^{10}\text{Be}$  + n). This calculation describes the wave function distortion of an initially bound particle as it passes by the potential induced by the reaction partner. This is performed in the framework of independent particles.

The wave function of the neutron halo is deduced from the potential found by N. Vinh Mau [10] to reproduce the inversion of the 2s and the 1p states in the  $^{11}\text{Be}$  nucleus for which a derivative of the Wood-Saxon potential is added at the surface. The potential reads

$$V_{Be}(r) = \frac{V_0}{1 + e^{\frac{r-R}{a}}} + 16.\alpha \frac{e^{2\frac{r-R}{a}}}{\left(1 + e^{\frac{r-R}{a}}\right)^4} \quad (1)$$

where the diffuseness  $a$  is 0.75 fm and the coefficient  $\alpha$  is equal to -10.56 MeV for the 2s state. The radius  $R$  equals to  $1.27 \times A^{1/3}$  fm. Numerically the initial wave-packet is obtained by diagonalizing the one-body Hamiltonian in spherical coordinates in a sphere of 30 fm radius with a space-step of  $\Delta r = 0.02$  fm. The depth  $V_0$  was taken to be -40 MeV. The wave function calculated in spherical coordinates for  $^{11}\text{Be}$  is then mapped onto Cartesian coordinates in order to calculate the dynamical evolution. Special attention has been given to the purity of the ground state  $^{11}\text{Be}$  neutron halo by performing an additional imaginary time evolution on the Cartesian network, after which the 2s state is found to be bound with -0.55 MeV.

The dynamical evolution of the system is given by the following single particle Schrödinger equation which reads in the  $r$  space

$$i\hbar \frac{d}{dt} \varphi(\mathbf{r}) = \left( \frac{-\hbar^2}{2m} \Delta + V_T(\mathbf{r} - \mathbf{r}_T(t)) + V_{Be}(\mathbf{r} - \mathbf{r}_{Be}(t)) \right) \varphi(\mathbf{r}) \quad (2)$$

where  $V_T$  and  $V_{Be}$  are the target and the projectile time-dependent potentials.  $\mathbf{r}_T(t)$  and  $\mathbf{r}_{Be}(t)$  correspond to the target and the projectile positions respectively. The nuclear potential of the target (Au, Ti or Be),  $V_T(\mathbf{r})$ , is taken to be of Wood-Saxon shape with a diffuseness  $a = 0.5$  fm, a radius  $R = 1.27A^{1/3}$  fm ( $A$  being the mass number of the Au, Ti or Be) and of depth adjusted to obtain the experimental binding energy of the last neutron. For the Au target,  $V_0 = -49.3$  MeV, giving a 3p state bound by about 8 MeV, for the Ti target,  $V_0 = -57$  MeV, giving a 1f state bound by about 11.6 MeV and for the Be target,  $V_0 = -40$  MeV, giving a 1p state bound by about 1.66 MeV.

In order to take into account the target and the  $^{10}\text{Be}$  core displacement, the evolution is performed for each time step using the classical Coulomb trajectory for the center of mass motions  $\mathbf{r}_T(t)$ ,  $\dot{\mathbf{r}}_T(t)$ ,  $\mathbf{r}_{Be}(t)$ ,  $\dot{\mathbf{r}}_{Be}(t)$  from a distance of -400 fm along the initial velocity axis between the projectile and the target and equal to the impact parameter  $b$  on the perpendicular axis.

The numerical method used for the trajectory calculation is the Runge-Kutta method. The split operator method [12] is used to solve the time dependent Schrödinger equation (Eq.2) with a time step of 1.7 fm/c on a mesh of  $64 \times 64 \times 64$  (fm<sup>3</sup>) with a step size of 0.5 fm. We have tested the numerical accuracy of the method with respect to the mesh parameters.

### III. RESULTS

#### A. Density plots

The result of these calculations (Fig.1) is presented for the  $^{11}\text{Be} + \text{Au}$  reaction as the wave-function density integrated over the  $z$ -axis,  $\rho_{2s}(x, y) = \int \phi(x, y, z)^2 dz$ , for impact parameters  $b = 10, 12, 15, 20$  and 40 fm, after the evolution of the 2s wave function initially in the  $^{10}\text{Be}$  potential.

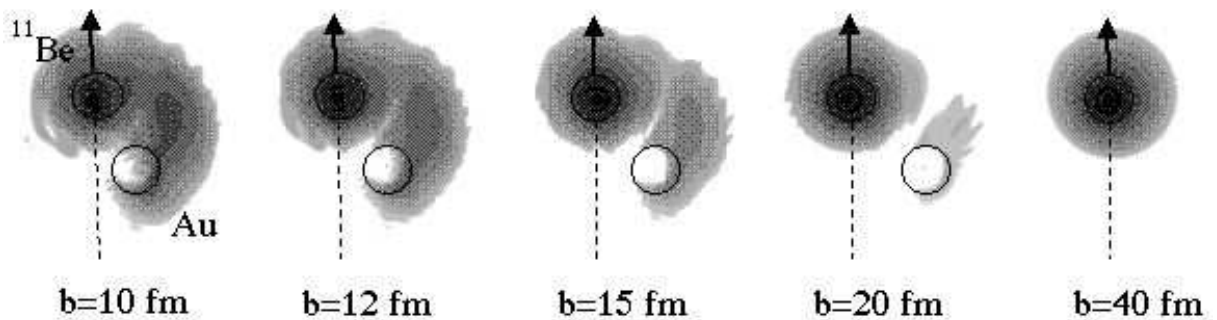


FIG. 1. Density plots of the 2s wave function in  $^{11}\text{Be}$  after scattering on a  $^{197}\text{Au}$  target for impact parameters of 10, 12, 15, 20 and 40 fm. The Coulomb trajectory is represented by the dashed line for each impact parameter. These plots are displayed in a logarithmic scale, black representing the most intense density. The ratio in density is 3 between each gray area.

After the evolution, we subtract the contributions of the wave-functions which are bound in the  $^{10}\text{Be}$  potential in order to keep only the emitted part of the wave-function. This subtraction is performed by projecting out all the bound states  $|\alpha\rangle$  of the neutron in the  $^{10}\text{Be}$ , leading to the emitted wave function  $|\psi\rangle$ .

$$|\psi\rangle = |\phi\rangle - \sum_{\alpha} |\alpha\rangle \langle \alpha | \phi \rangle \quad (3)$$

The bound wave functions in the  $^{10}\text{Be}$  core potential are the 2s state itself bound by -0.55 MeV, the 1s state bound by -23 MeV and the 1p state using the same nuclear potential and which is then bound by about -11 MeV. Fig.2 shows the same evolutions as Fig.1 after the subtraction of these components. A sizeable fraction of the wave function is then removed around the  $^{10}\text{Be}$  core position.

One can see that the small impact parameters ( $b \leq 20$  fm) are responsible for large angle neutron emission. For larger impact parameters, neutrons are forward focussed. This small angle emission can be understood as a Coulomb dissociation in which the  $^{10}\text{Be}$  core has been shaken by the Coulomb field of the target. In our calculation, for large impact parameters, we observe a displacement of the neutron wave function compared to the core which might be the first oscillation of a soft dipole resonance as it has been suggested in ref. [13]. Due to the weak binding of the last neutron, the halo has separated from the core, transferring little momentum to the neutron which is then emitted along the initial trajectory.

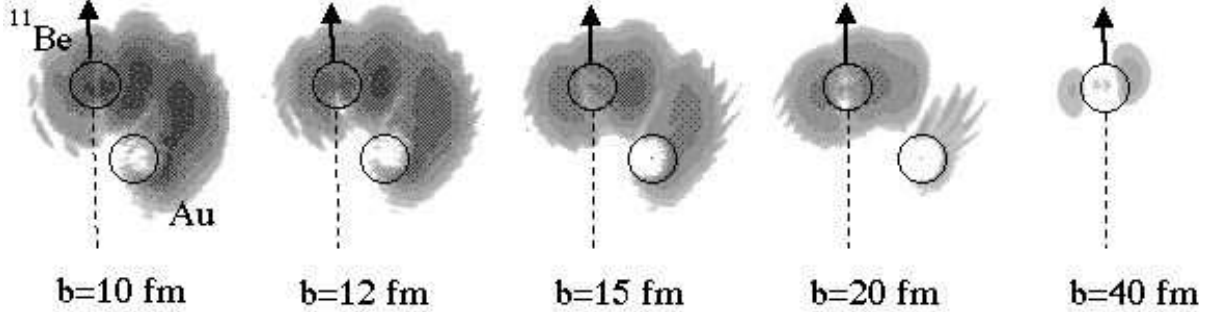


FIG. 2. Density plots of the 2s wave function of  $^{11}\text{Be}$  after scattering on a  $^{197}\text{Au}$  target with an impact parameter of 10, 12, 15, 20 and 40 fm and after subtraction of the bound wave functions.

The calculation shows a weak emission (see Fig.2 right) which must, however, be integrated over a large impact parameter domain to obtain the total cross section.

In order to compute cross-sections, we used the following method. For large impact parameters the fraction of wave function emitted is small and thus according to the perturbation theory, to gain time and reduce the error inherent to the method, we performed the calculation up to the minimum distance of approach and multiplied the result by two. On the contrary, for small impact parameters (below 20 fm) the nuclear break-up cross section is much larger than the Coulomb break-up cross section as will be shown in section B. As this nuclear potential spreads the wave function on the whole mesh (see Fig.1 and 2) we stopped the calculation at a distance of 20 fm after the projectile has passed by the target and checked that the extracted values do not change for a slightly longer evolution.

### B. Interplay between nuclear and Coulomb break-up.

Since the  $^{10}\text{Be}$  core is detected in the experiment, we assumed a minimum impact parameter corresponding to a grazing trajectory. We followed the strong absorption model for which the minimum parameter is calculated as  $1.4(A_T^{1/3} + A_{Be}^{1/3})$  fm yielding to  $b_{min} = 11$  fm for the Au target,  $b_{min} = 8$  fm for the Ti target and  $b_{min} = 6$  fm for the Be target. To obtain a total cross section, this calculation was performed for impact parameters running from the grazing parameter, to an impact parameter where the fraction of wave function emitted no longer changes with increasing impact parameter. This is shown in Fig.3 where the fraction of wave function emitted  $Frac = \int d^3r |\psi|^2$  is plotted versus the impact parameter.

For the Au target this percentage starts to saturate around 200 fm whereas for the Ti it is around 100 fm and 40 fm for the Be target. At these impact parameters the fraction of wave function emitted is around 0.04%. At the saturation, only the noise inherent to the numerical method remains and we do not include larger impact parameters in the cross section estimate.

In this figure we clearly see a change in the dependence of  $Frac$  on impact parameter, between the small and the large impact parameters which could indicate the transition between the nuclear and the Coulomb perturbation.

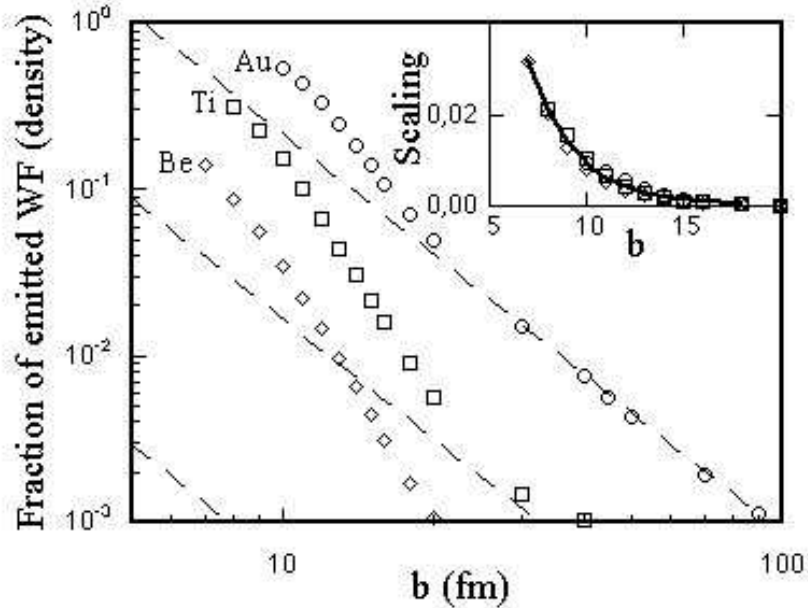


FIG. 3. Fraction of wave function emitted ( $Frac$ ) versus the impact parameter for the three targets (symbols). Dashed lines are fits obtained with the formula  $\alpha b^\beta$  for the large impact parameters (see text). Inset: scaling of  $Frac - \alpha b^\beta$  with  $A_T^{2/3}$  (symbols). The solid line is the fit of the scaling with  $e^{-\gamma b}$  (see text).

In order to get a deeper insight in the interplay between nuclear and Coulomb break-up, we have studied the mass and charge dependence of the fraction emitted ( $Frac$ ) with the impact parameter. At large impact parameter, above 40 fm, the wave function does not see the target nuclear potential and only the Coulomb field is felt by the core. We have fitted  $Frac$  for the Au and Ti targets at large impact parameters with the formula  $\alpha b^\beta$ . We found  $\beta = -2.4$  and  $\alpha$  which scales quadratically with the charge as  $\alpha = 0.0088 \times Z^2$ . Fits are shown on Fig.3 as dashed lines (we assumed the same dependence for the Be target). The scaling with the charge observed for the Au and Ti targets clearly demonstrates that large impact parameters can be described by a perturbative Coulomb dissociation.

We extrapolated the Coulomb effect to the small impact parameters and by subtracting the fit curve to the fraction emitted we obtained a function which we expect to only contain the nuclear effect. Indeed, after renormalizing these results with  $A_T^{2/3}$ , we obtained a quantity named  $Scaling = (Frac - \alpha b^\beta)/A_T^{2/3}$ , which no longer depends on the target (see insert of Fig.3). This leads to a cross section that scales with  $A_T^{2/3}$  as expected for the nuclear emission [14]. This curve can be fitted in turn by an exponential decay which is typical of a transmission mechanism ( $Scaling \propto e^{-\gamma b}$  with  $\gamma = 0.40 \pm 0.01 \text{ fm}^{-1}$ ).

We would like to emphasize that this empirical fitting method indicates a rather good separation between Coulomb and nuclear effects in our calculation. Such a separation, which comes as an hypothesis in perturbative framework, is however not natural in our framework where both effects are accounted for at the same time and can therefore interfere.

Using the parameters extracted from the fits and integrating over the impact parameter, we extract the variation of the break-up cross section with the charge of the target for both the Coulomb and the nuclear interactions. This evolution is presented in Fig.4. We observe a Coulomb cross section that scales with  $Z^{1.65}$  close to the value of 1.725 from ref. [15].

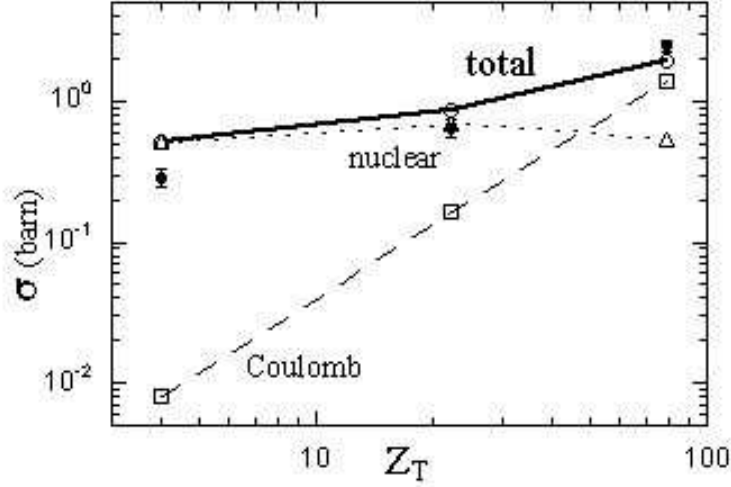


FIG. 4. Coulomb (squares) and nuclear break-up (crosses) cross sections as a function of the target charge ( $Z_T$ ) obtained from the fits to the calculated fraction of the wave function emitted and the fit to the Scaling parameter, integrating from the corresponding  $b_{min}$ . The Coulomb contribution scales with  $Z_T^{1.65}$  (not shown in the figure). The total cross-section (Coulomb+nuclear) is also reported as circles joined by a plain line and compared to the experimental data (diamonds with error bars) of ref. [3].

It should be noticed that in the case of the Au target we have checked this analysis by turning on and off the nuclear and the Coulomb field separately in the calculation.

### C. Cross sections and angular distributions

Once we have the fraction of wave-function emitted we can access the differential cross-section by integrating the corresponding probability between  $b_{min}$  and  $b_{max}$  defined in previous section. For each impact parameter  $b_n$  (fm), the cross section is equal to  $2\pi b_n \Delta b_n \cdot 10^{-2}$  (barn) times the square of the fraction of wave function which is emitted, where  $\Delta b_n$  is taken to be equal to  $(b_{n+1} - b_{n-1})/2$ . The step in impact parameter between two calculations varied from 1 fm (for small impact parameters) to 40 fm above  $b = 150$  fm.

The angular distribution of the emitted neutron is extracted by applying the Fourier transform to obtain the remnant part of the wave function in the momentum space (Fig.5).

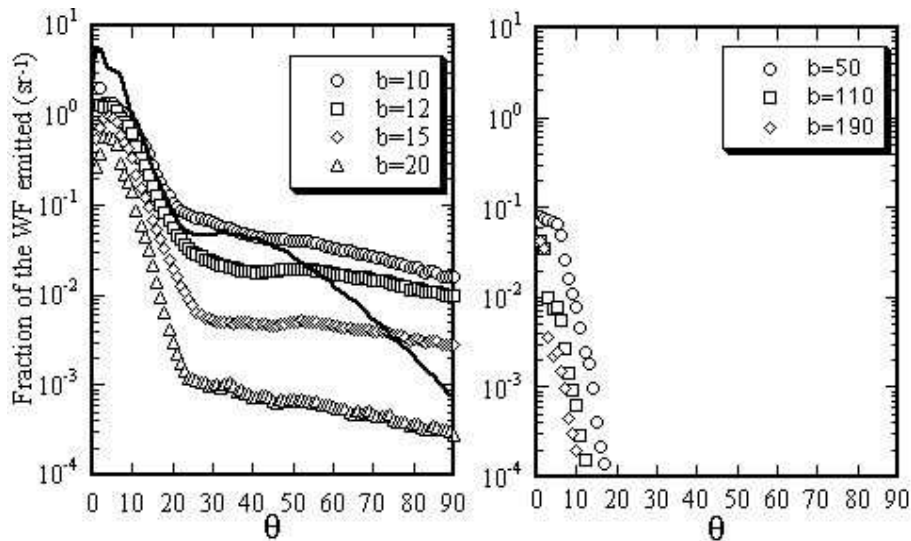


FIG. 5. Angular distributions of the fraction of the wave function emitted for impact parameters from 10 to 20 fm (left) and from 50 to 190 fm (right). On the left figure the Fourier transform of the initial 2s wave function is also shown as a plain line.

For small impact parameters, nuclear effects become important and the nuclear refraction of the neutron halo gives rise to an emission at large angles. This can be seen in the spectra extracted from the calculations performed at impact parameters of 10 to 20 fm which exhibit a component at angles above 30 degrees. This emission to the continuum is known as Towing Mode. In that case, a nucleon from the target is pulled out, towed along by the projectile and finally expelled at large angles and large velocities in the laboratory frame [9]. In the case of the  $^{11}\text{Be}$  experiments, the emitted neutron belongs to the projectile (the  $^{11}\text{Be}$ ) which breaks up as it is perturbed by the target nuclear potential. In the  $^{11}\text{Be}$  frame, this nuclear break-up can be seen as the emitted neutron being accelerated by the target potential (see Fig.2). We expect the same mechanism to be present for this halo nucleus as for a stable nucleus. However, in the case of a halo nucleus, the cross section of this nuclear break-up should be increased compared to a stable nucleus, due to the large extension of the neutron wave function and thus the larger impact parameter at which it sees the nuclear potential of the other nucleus. This will be discussed further when comparing with a more bound wave function (see section D).

At larger impact parameters, above 50 fm, only the component between 0 and 15 degrees remains (Fig.5 right). There, the neutron wave function does not feel the nuclear potential anymore and the break-up comes from the deviation of the  $^{10}\text{Be}$  core in the Coulomb field. Indeed, because the halo neutron of  $^{11}\text{Be}$  is so weakly bound, a light shaking of the core is enough to induce the break-up. This, in turn, is not expected with a more strongly bound nucleus as it will be discussed further in section D.

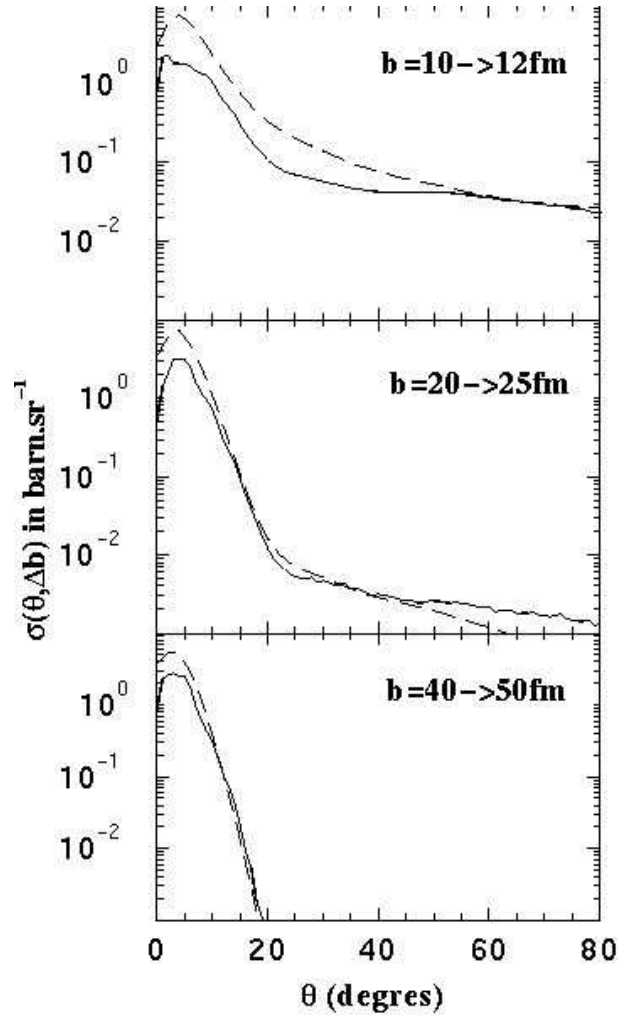


FIG. 6. Angular distribution for the emission of the  $^{11}\text{Be}$  halo neutron using a perturbative approach (dashed lines) and our calculation (plain lines) for three regions of impact parameter.

We have compared our calculation with a perturbative approach proposed by Bonaccorso, Brink and Margueron presented in ref. [5,16] (called here perturbative). For this perturbative calculation, we imposed an imaginary optical potential equal to zero and took for the real part the same optical potential as for the non-perturbative calculation presented here. The wave function of the neutron halo is taken as the outer part of a 2s wave-function and normalized to the wave function used in our dynamical evolution. At small impact parameters we know that a large fraction of the wave function is emitted (Fig.3 shows that more than 70% of the wave function is emitted for 10 fm of impact parameter) which indicates that the perturbative approach is not adequate, however at large impact parameters this value becomes small (5% at 50 fm of impact parameter) and there the perturbative approach is well justified. We thus expect the results of our calculations to be different from the perturbative approach for small impact parameters and to become more and more similar as we go at larger impact parameters. Fig.6 shows this comparison for three regions of impact parameters for the break-up on a Au target.

For the region between 10 and 12 fm the two calculations predict a quite different shape of the neutron angular distribution. At large impact parameter, the two calculations exhibit similar shapes of the neutron angular distributions. The larger cross section observed around 5 degrees in the perturbative approach, can be traced back to the difference in the calculated wave function which in the case of the perturbative calculation increases exponentially in the inner part of the nucleus.

#### D. Comparison between halo and non-halo neutron emissions

Our calculation has also been performed to infer the evolution of a strongly bound wave function. We used a Wood-Saxon potential with  $V_0=-70.5$  MeV,  $A=11$ , and obtained a 2s wave function bound by 7 MeV. The calculation has been performed for a Au target and for impact parameters running from 10 fm to 110 fm. The result is shown in Fig.7 and is compared to the break-up of the  $^{11}\text{Be}$  halo for the same impact parameter range. The differential cross section of neutron emission for the bound nucleus is more than hundred times lower than for  $^{11}\text{Be}$  below 10 degrees. For large angles, around 40 degrees, the differential cross section is about 4 times lower. This latter difference can be understood by the extension of the wave function, which is much larger in case of a halo.

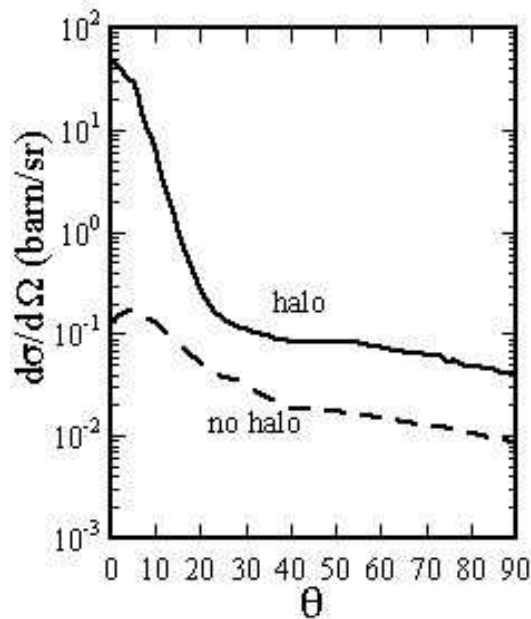


FIG. 7. Angular distribution for the emission of the  $^{11}\text{Be}$  halo neutron (plain line) and a non-halo neutron (dashed line) bound by 7 MeV after the scattering on a Au target summed over impact parameters between 10 fm and 110 fm.

In particular, it is often argued that Coulomb effects shadow the nuclear mechanism in heavy targets like Au. Although the relative proportion of these two effects is largely in favor of Coulomb dissociation, we show that nuclear break-up is of major importance for large angle emission. Whereas Coulomb dissociation on a heavy target such as Au could be a direct measurement of the binding energy of the particle, nuclear diffraction could in turn bring information on the extension of the wave function, and hence answer the question whether we are dealing with a halo

state or not. Furthermore, in stable nuclei, it has been shown that transfer to the continuum due to a mechanism such as the Towing Mode might be a tool to infer information on shell structure as presented in ref. [9]. One might then be able to use this large angle emission to obtain additional information on nuclear halo wave-function properties.

### E. Comparison with the $^{11}\text{Be}$ data

To compare our calculation to the data of ref. [3], we extracted the differential cross section by summing the calculations from  $b_{min}$  up to  $b_{max}$ . For the Au target we took  $b_{max} = 210$  fm, 120 fm for Ti and 40 fm for Be. Calculations are shown in Fig.8, multiplied by 0.84 to take into account the spectroscopic factor of the 2s state found experimentally and reported in ref. [11]. The calculation is compared to the experimental data of ref. [3] for all three targets taking into account the experimental threshold of 26 MeV for the neutron detection. Note that our calculation includes all the inelastic channels in which the target is excited but also those in which the  $^{10}\text{Be}$  remnant is in an excited state below its neutron separation energy. This is also included in the data that measure the  $^{10}\text{Be}$  and the neutron. However our calculation does not take into account the possible two body dissipation since we use a single-particle framework. The calculations are in good agreement with the experimental data, both at small and large angles. The simultaneous reproduction of data for the Au and the Be targets demonstrates that the Coulomb and the nuclear interactions are well taken into account. The agreement with the Ti target data is of lower quality, however the data show large error bars for the cross section of neutrons emitted above 15 degrees. Finally the possible contribution of a neutron in a 1d state coupled to a 2+ excitation of the core as deduced from the experiment [11] has not been calculated so far. However, since we already reproduce the whole cross section for the Au target with 84% of the 2s break-up, the contribution of the 1d state would seem to be small in this case.

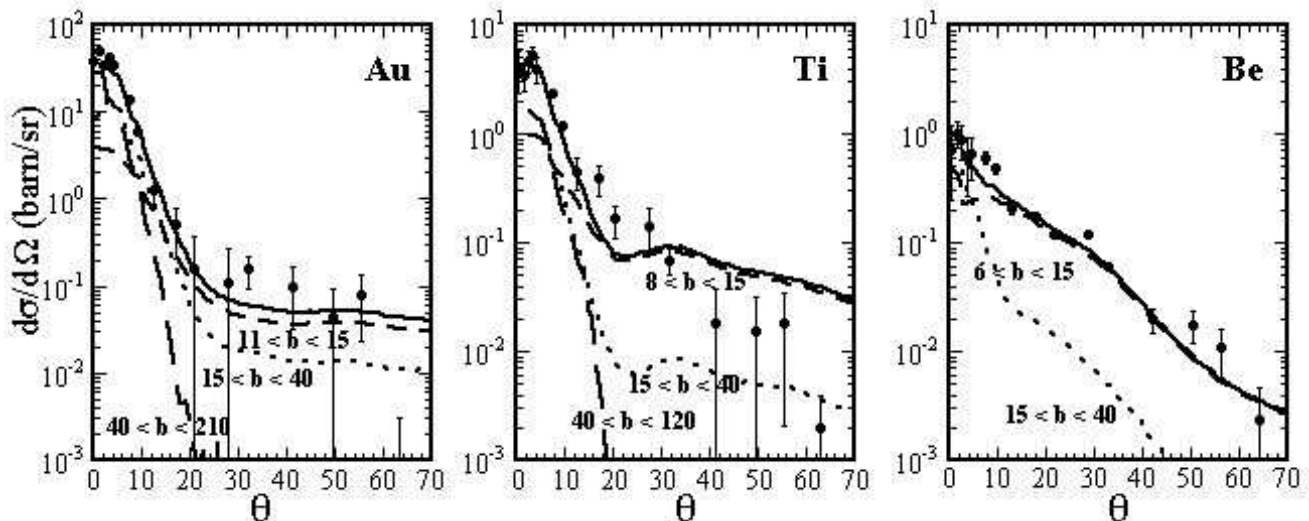


FIG. 8. Calculated angular distributions for impact parameter running from  $b_{min}$  to  $b_{max}$  (11 to 210 fm for the Au target (left figure)) (plain line) for neutron of energy higher than 26 MeV. Dots with error bars are data points from ref.[3]. Middle figure is for the Ti target and right figure for the  $^9\text{Be}$  target. Contribution of the calculation for three impact parameter regions,  $b_{min}$  to 15 fm (short dashed lines), 15 to 40 fm (dotted lines) and 50 to  $b_{max}$  (long dashed lines) are also presented.

## IV. CONCLUSION

We have investigated the neutron break-up of a halo nucleus in the reactions Au, Ti, Be ( $^{11}\text{Be}$ ,  $^{11}\text{Be}+n$ ) at 41 MeV per nucleon, in the framework of a time dependent quantum model. Results were compared with the experimental neutron angular distributions of Ref. [3] and a good agreement was found. Our calculation, that includes both the Coulomb and the nuclear interactions, confirms that the forward peaked neutrons are due to the Coulomb break-up and that the neutrons emitted at large angles come from the interaction of the halo neutron with the target nuclear potential. This diffractive mechanism is called towing mode [9]. A strong angular correlation between the towed particle and the projectile was observed in reaction between stable nuclei and is also expected for the  $^{11}\text{Be}$  break-up. However the experiments performed so far did not measure the scattering angle of the remnant  $^{10}\text{Be}$ . Our calculations

show that neutron emitted below 15 degrees arise from the Coulomb dissociation and most of the cross section comes from large impact parameters as the neutron halo of  $^{11}\text{Be}$  is weakly bound. The shaking of the  $^{10}\text{Be}$  core by the Coulomb field leads to the dissociation of the halo and the emission of the neutron in the forward direction. This can also be understood as a Coulomb excitation of  $^{11}\text{Be}$  above the particle threshold, followed by neutron emission. This is the only mechanism contributing to the break-up when the impact parameter is such that the halo wave function does not overlap with the nuclear perturbative potential. The Coulomb break-up is very much hindered for strongly bound neutrons, whereas the nuclear break-up decreases by a factor of four due to the lesser extension of the wave function. Calculations for the 1d wave function should be performed for the  $^{11}\text{Be}$  break-up to infer its contribution and understand better the data. More generally, those calculations could be used to extract information on the wave function of the last bound neutron for unstable nuclei for which the properties is not well known yet, provided that a measurement of the neutron angular distribution cross section is performed both at large and small angles.

---

- [1] I. Tanihata et al, Phys. Rev. Lett. 55 (1985) 380. I.Tanihata, J. Phys. G22 (1996) 157.
- [2] P.G. Hansen, A.S. Jensen and B. Jonson, Annu. Rev. Nucl. Part. Sci. 45 (1995) 591.
- [3] R.Anne et al., Nucl. Phys. A575 (1994) 125.
- [4] A.Bonaccorso, D. Brink Phys. Rev. C 57 (1998) 22.
- [5] A.Bonaccorso, D. Brink Phys. Rev. C 58 (1998) 2864.
- [6] V.S.Melezhik and D.Baye Phys. Rev. C 59, (1999) 3232.
- [7] S.Typel and H.H.Wolter, Z.Naturforsch. 54A, (1999) 63.
- [8] D.Lacroix, J.A.Scarpaci and Ph.Chomaz, Nucl. Phys. A 658 (1999) 273.
- [9] J.A.Scarpaci et al., Phys. Lett. B 428 (1998) 241.
- [10] N.Vinh Mau, Nucl. Phys. A 592 (1995) 33.
- [11] S.Fortier et al., Phys. Lett. B461, 22 (1999).
- [12] M.D.Feit, J. Fleck, Jr. and A. Steiger, J. Comput. Phys. (1982) 412; M.D. Feit and J.A. Fleck, Jr., J. Chem. Phys. **78** (1983) 301; *ibid.*, **80** (1984) 2578.
- [13] T.Nakamura et al., Phys. Lett. B331, (1994), 296.
- [14] T.Kobayashi et al, Phys.Lett. B232 (1989) 51.
- [15] P.G.Hansen and B.Jonson, Europhys.Lett. 4 (1987)409.
- [16] A.Bonaccorso, J.Margueron and D.Brink, to be published.